Experimental Mechanics
https://doi.org/10.1007/s11340-023-01016-y

RESEARCH PAPER

A Thermodynamic Framework for Rapid Prediction of S-N Curves Using Temperature Rise at Steady-State

A. Mahmoudi[1] · **M.M. Khonsari**[1]

Received: 13 June 2023 / Accepted: 3 November 2023
© Society for Experimental Mechanics 2023

Abstract

Background Building S-N curves for materials traditionally involves conducting numerous fatigue tests, resulting in a time-consuming and expensive experimental procedure that can span several weeks. Thus, there is a need for a more efficient approach to extract the S-N curves.

Objective The primary purpose of this research is to propose a reliable approach in the framework of thermodynamics for the rapid prediction of fatigue failure at different stress levels. The proposed method aims to offer a simple and efficient means of extracting the S-N curve of a material.

Methods In this paper, a method is introduced based on the principles of thermodynamics. It uses the fracture fatigue entropy (FFE) threshold to estimate the fatigue life by conducting a limited number of cycles at each stress level and measuring the temperature rise during the steady-state stage of fatigue.

Results An extensive set of experimental results with carbon steel 1018 and SS 316 are conducted to illustrate the utility of the approach. Also, the efficacy of the approach in characterizing the fatigue in axial and bending loadings of SAE 1045 and SS304 specimens is presented. It successfully predicts fatigue life and creates the S-N curves.

Conclusion The effectiveness of the approach is evaluated successfully for different materials under different loading types. The results show that the temperature rise is an indicator of the severity of fatigue and can be used to predict life.

Keywords Fracture Fatigue Entropy (FFE) · Thermography · S-N curve · Fatigue degradation · Self-heating

Nomenclature

A	Conjugated force of internal variable
A_{cond}	Cross-sectional area
A_{surf}	Surface area
c_p	Specific heat capacity
e	Specific internal energy
$\dot{E}_{diss}$	Rate of dissipated energy
$\dot{E}_{gen}$	Rate of internal energy generation
$\dot{E}_{in}$	Rate of energy entering the material
FFE	Fracture fatigue entropy
h	Heat transfer coefficient
k	Thermal conductivity
m	Material Constant
N_f	Number of cycles to failure
$\vec{q}$	Heat flux across the boundary
R_θ	Rate of temperature rise at the beginning of the fatigue process
s	Specific entropy
t	Time
T	Temperature
T_s	Steady-state temperature
V	Volume of the gauge section
V_k	Internal variable
W_P	Mechanical dissipation due to plastic deformation
$\dot{W}_t$	Rate of total energy generation
γ	Non-negative entropy generation
γ_f	Entropy generation up to fracture
$\dot{\epsilon}$	Total strain rate
ϵ^e	Elastic strain
ϵ^p	Plastic strain
ρ	Density
σ	Symmetric stress tensor
ψ	Helmholtz free energy
θ	Temperature rise of gauge section (The difference between gauge section and remote area)
θ^d	Temperature rise due to damaging energies

✉ M.M. Khonsari
khonsari@lsu.edu

[1] Department of Mechanical and Industrial Engineering, Louisiana State University, Baton Rouge, LA, USA

Published online: 28 November 2023

θ^{nd} Temperature rise due to non-damaging energies
Δz Distance between gauge section and grips

Introduction

Mechanical components undergoing cyclic loading are vulnerable to degradation and fatigue failure [1]. It is widely acknowledged that when components are externally actuated, they generate unrecoverable heat, resulting in self-heating and an increase in temperature. Extensive experimental studies have established a direct correlation between the applied load and the rise in surface temperature [2]. Consequently, temperature fluctuations during cyclic loading have been extensively employed to assess the extent of fatigue degradation [3, 4]. Evaluating the heat production during fatigue is a method for assessment of fatigue degradation. Luong [5] used an energetic approach to correlate the heat production and intrinsic dissipation mechanisms in the material. Boulanger et al. [6] proposed a thermodynamic framework to determine the heat source from temperature response during fatigue. They showed that heat dissipation is in direct relation with stress amplitude and frequency. Morabito et al. [7] and Chrysochoos et al. [8] utilized heat diffusion equations to quantify the dissipative heat sources. Although these methods require a great deal of data, they provide useful information about thermoelastic sources and damage evolution during fatigue.

In general, when a material undergoes fatigue, the surface temperature tends to rise rapidly during the initial stages of the fatigue process. Subsequently, it reaches a steady-state temperature that persists for most of the fatigue duration until a sudden increase occurs near the fracture point [3]. Numerous researchers have capitalized on this temperature pattern to investigate the behavior of metal fatigue. By leveraging the temperature variations during the fatigue process, one can gain valuable insights into the characteristics of fatigue in metallic materials [9–11]. La Rosa and Risitano [12] proposed a method for rapid evaluation of the fatigue limit of mechanical components by conducting a limited number of tests. Guglielmino et al. [13] proposed a method based on energetic release during a tensile test to assess the fatigue properties of a material. Palumbo and Galietti [14] used the thermoelastic signal as a parameter to evaluate the fatigue damage and predict the fatigue limit of welded joints. Finis et al. [15] developed a data analysis procedure to evaluate the thermographic signals in order to estimate the fatigue limit of stainless steels.

On the other front, recent advances in infrared thermography have incentivized researchers to develop a thermodynamics framework for understanding fatigue as an irreversible process of damage accumulation. This framework applies to both metallic and non-metallic materials [16–21]. This approach considers the temperature changes observed during fatigue and incorporates them into a broader understanding of the underlying thermodynamic principles governing the progressive degradation of materials [22–24].

In the present study, we propose a method that directly uses the temperature rise to quantify the energy dissipation and correlates the plastic strain energy with the steady-state temperature rise. The concept of fracture fatigue entropy (FFE) is then utilized as a failure criterion to efficiently construct the S-N curve. The damaging and non-damaging parts of energy production and temperature rise are evaluated for accurate prediction of fatigue limit and fatigue life at different stress levels. An extensive set of experimental results is presented to investigate the efficacy of the proposed method to rapidly predict the S-N curve for different materials.

Theory and Formulation

First and Second Laws of Thermodynamics

Fatigue represents an irreversible degradation process characterized by the dissipation of heat [23]. Consequently, the study of internal heat generation and temperature fluctuations during cyclic loading necessitates the application of a thermodynamic framework. The first law of thermodynamics for a material undergoing fatigue and subjected to small deformations can be written in terms of specific quantities as [25]:

$$\rho\dot{e} = \sigma\colon \dot{\varepsilon} - div\vec{q} \tag{1}$$

where ρ represents density, e is the specific internal energy, and $\sigma\colon \dot{\varepsilon}$ is the energy generation due to mechanical work. σ denotes the applied stress and $\dot{\varepsilon}$ is the total strain rate ($\dot{\varepsilon} = \dot{\varepsilon}_e + \dot{\varepsilon}_p$), where ε_e and ε_p are the elastic and plastic strains, respectively. $\vec{q}$ is the heat flux across the boundary.

The second law of thermodynamics states that the entropy generation during a process is always non-negative as:

$$\rho\frac{ds}{dt} \geq -div\frac{\vec{q}}{T} \tag{2}$$

where s and T are the specific entropy and temperature, respectively. Helmholtz free energy (HFE), $\psi = e - Ts$, relates the first and second laws of thermodynamics to each other. It is a function of state variables as $\psi = \psi(\varepsilon, \varepsilon^e, \varepsilon^p, T, V_k)$, where V_k are internal state variables. Using the ψ function and combining equations (1) and (2) yields [25]:

$$\frac{\sigma\colon \dot{\varepsilon} - \rho\left(\dot{\psi} + s\dot{T}\right) - \frac{\vec{q}.\nabla T}{T}}{T} \geq 0 \tag{3}$$

Noting that $\varepsilon_e = \varepsilon - \varepsilon_p$, the HFE function can be reduced to $\psi = \psi(\varepsilon^e, T, V_k)$. Differentiation of ψ with respect to time yields:

$$\frac{\partial \psi}{\partial t} = \left(\frac{\partial \psi}{\partial \varepsilon_e}\right) : \dot{\varepsilon}_e + \left(\frac{\partial \psi}{\partial T}\right) : \dot{T} + \left(\frac{\partial \psi}{\partial V_k}\right) : \dot{V}_k \tag{4}$$

Substituting equation (4) into equation (3), the second law of thermodynamics is expressed by the following equation:

$$\dot{\gamma} = \frac{\sigma : \dot{\varepsilon}_p}{T} + \frac{A\dot{V}_k}{T} - \frac{\vec{q}.\nabla T}{T^2} \geq 0 \tag{5}$$

where $\dot{\gamma}$ is the non-negative entropy generation rate and A is the thermodynamic force associated with the internal state parameter V_k.

Applying Fourier's law, $\vec{q} = -k\nabla T$, specific heat relationship with temperature and entropy, $c_p = T\,\partial s/\partial T$, and the thermodynamic forces associated with the strain and temperature, $\sigma = \rho\,\partial \psi/\partial \varepsilon$ and $s = -\partial \psi/\partial T$, the first law of thermodynamics (equation (1)) can be written as:

$$\rho c_p \dot{T} = \sigma : \dot{\varepsilon}_p + A\dot{V}_k + k\nabla^2 T \tag{6}$$

where k is the material's heat conductivity coefficient. The energy associated with the internal parameters ($A\dot{V}_k$) in metal is only 5–10% of plastic strain energy ($\dot{W}_p = \sigma : \dot{\varepsilon}_p$) [26] and can be neglected. Also, it is shown that entropy generation owing to heat conduction, the last term in equation (5), is negligible [23, 27]. Therefore, the entropy generation associated with the damaging energies can be obtained as:

$$\gamma_f = \int_0^{t_f} \frac{\dot{W}_p}{T} dt = \int_0^{t_f} \frac{\sigma : \dot{\varepsilon}_p}{T} dt \tag{7}$$

Evolution of Temperature

A typical IR camera recording in Fig. 1 illustrates the characteristic temperature evolution pattern observed during the fatigue process of SS 316 specimens at a stress amplitude of 320 MPa. In this figure, θ represents the temperature rise and $R_\theta = d\theta/dt$ is the rate of temperature rise at the beginning of the fatigue test. Initially, the temperature rises rapidly at the onset of cyclic loading (Phase I) where the rate of temperature rise decreases. The first phase is followed by a stabilization phase (Phase II) for most of the fatigue process where the rate of temperature rise is nearly constant. Finally, a sudden temperature increase occurs just before fracture where the rate of temperature rise also sharply increases (Phase III). This 3-stage temperature trend is a well-known pattern in fatigue dissipation [12].

The first law of thermodynamics, the conservation of energy in equation (6), can be rewritten in terms of energy generation and dissipation as:

$$\dot{E}_{in} + \dot{E}_{gen} = \rho c_p \frac{dT}{dt} + \dot{E}_{diss} \tag{8}$$

Equation (8) states that energy entering material ($\dot{E}_{in}$) and internal energy generation ($\dot{E}_{gen}$) contribute to the increase in temperature ($\rho c_p \frac{dT}{dt}$) and the portion of heat that is dissipated to the environment ($\dot{E}_{diss}$) via conduction, convection or radiation. In a cyclic loading process, the internal heat generation is the result of plastic and inelastic deformations inside the material [28], so that $\dot{E}_{gen}$ in equation (8) accounts for self-heating in the material due to external actuation and $\dot{E}_{gen} = \dot{W}_t$. Typically, no heat enters the control volume ($\dot{E}_{in} = 0$) and the radiation to the environment is negligible due to relatively low surface temperature. It can be shown that equation (8) is reduced to the heat conduction in a one-dimensional direction and can be written as follows [29]:

$$\dot{W}_t = \rho c_p \frac{dT}{dt} + k\frac{A_{Cond}}{V}\frac{(T - T_\infty)}{\Delta z} + h\frac{A_{Surf}}{V}(T - T_\infty) \tag{9}$$

where V is the volume of the gauge section, and A_{Cond} and A_{Surf} represent the cross-sectional area and surface area,

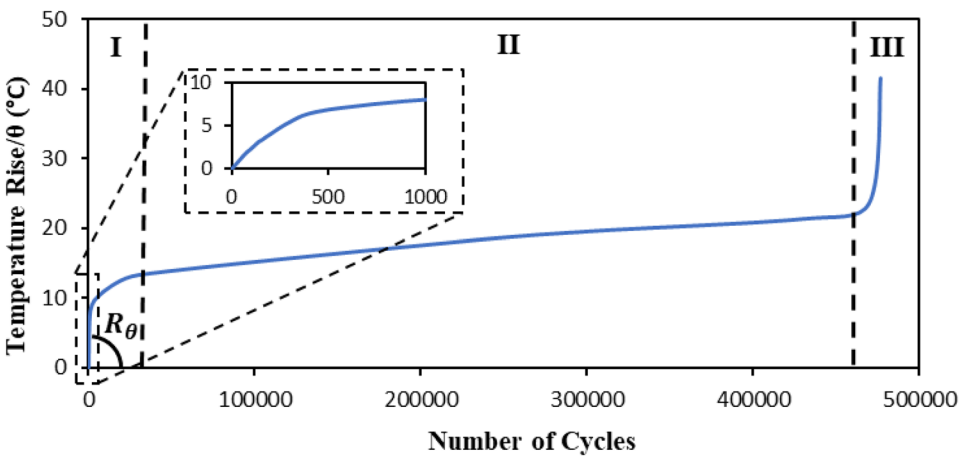

Fig. 1 Temperature evolution of SS316 specimen at 320 MPa at different phases of the fatigue process

respectively. Δz denotes the distance of the gauge length to the machine grips, which is assumed to have the constant temperature of the environment, T_∞. Using the variable change of $\theta = T - T_\infty$, equation (9) yields to:

$$\frac{d\theta}{dt} + m\theta = \frac{\dot{W}_t}{\rho c_p} \tag{10}$$

where $m = \frac{hA_{Surf}}{\rho c_p V} + \frac{kA_{Cond}}{\rho c_p V \Delta z}$.

At the beginning of the fatigue test $\theta = 0$, and at the steady-state phase $d\theta/dt = 0$. Thus, for these two specific moments, $\dot{W}_t$ can be obtained as:

$$\dot{W}_t = \begin{cases} \rho c_p R_\theta, & \text{at the beginning of the fatigue process} \\ m\rho c_p \theta, & \text{at steady state} \end{cases} \tag{11}$$

It has been shown that in low-cycle fatigue, the plastic strain energy, $\dot{W}_p$, is the dominant mechanism for internal heat generation [28] while in high-cycle fatigue the internal friction is significant and should be considered as discussed in the next section.

Life Prediction Using Temperature Rise

Extensive research shows that the capacity of entropy accumulation up to fracture is a material property and a constant parameter called fracture fatigue entropy (FFE) [30]. This parameter is independent of the type of loading (e.g., tension-compression, bending, torsion) and specimens' types and sizes and can be calculated using equation (7). Considering that most of fatigue life is expended in the steady-state stage, FFE can be calculated as:

$$FFE = \frac{N_f \dot{W}_p}{fT_s} \tag{12}$$

where N_f, f and T_s are the number of cycles to failure (fatigue life), frequency of loading, and stabilized temperature, respectively. In low-cycle fatigue (LCF), the plastic strain energy, $\dot{W}_p$, is the dominant mechanism of internal heat generation and can be replaced by $\dot{W}_t$ from equation (11). For high-cycle fatigue (HCF), The portion of temperature rise related to the damaging mechanisms should be determined. According to [31], the portion of the non-damaging energies in total internal heat generation can be obtained using the change of slope in the graph of temperature rise versus stress depicted in Fig. 2. The damaging mechanisms, including microplasticity, occur for stress levels above the fatigue limit and cause inelastic energy dissipation, while the heat generation below the fatigue limit is due to internal friction between grain boundaries and is non-damaging energy [32, 33]. Referring to Fig. 2, as the fatigue stress increases, the microplasticity and crack nucleation occur at stress levels above the fatigue limit, where the rate of steady-state temperature rise changes. Thus, it can be stated that, in general, the temperature rise at a steady state emerges from two sources. The first part is related to non-damaging energies (θ^{nd}) and the second part is related to damaging energies (θ^d). Using equation (11), if θ^d is known, FFE can be calculated as:

$$FFE = N_f m \rho C_p \frac{\theta^d}{fT_s} \tag{13}$$

Equation (13) can be utilized to predict fatigue life (N_f) using the stabilized temperature by solving the following equation:

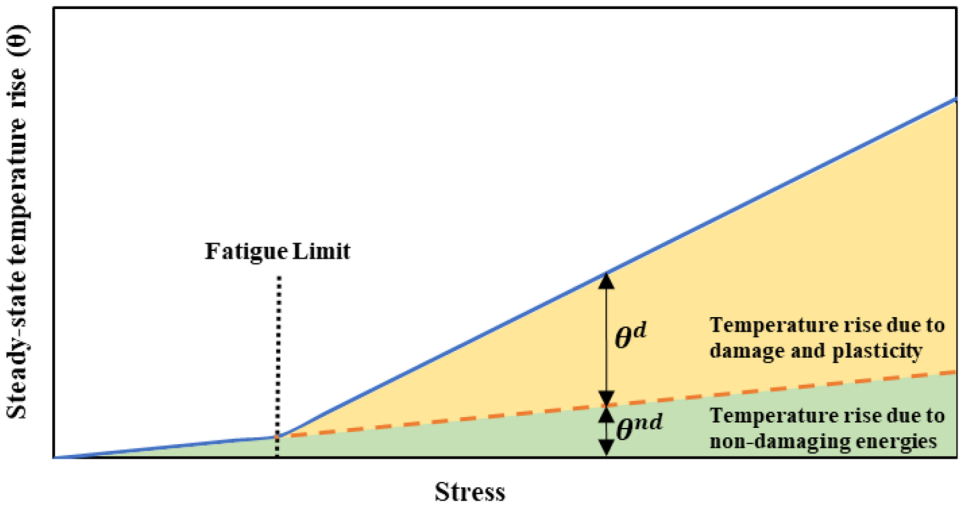

Fig. 2 Schematic of steady-state temperature rise at different stress levels

Table 1 The chemical composition of CS 1018 and SS 316

Material	C	Fe	Mn	S	P	Cr	Mo	Si	Ni
CS 1018	0.14–0.2	98.81–99.26	0.6–0.9	0.05 Max	0.04 Max	-	-	-	-
SS 316	0.08	82 Max	-	0.03	0.045	18 Max	3 Max	1	14 Max

$$N_f = \frac{FFE}{m\rho C_p}\frac{fT_s}{\theta^d} \tag{14}$$

One of the applications of this approach is to construct the S-N curve of material by only running a few load cycles to reach the steady-state phase of fatigue. In this approach, if a fatigue life at a stress level is experimentally determined, the stabilized temperature of other stress levels can be used to find the corresponding life without necessarily bringing the fatigue test to fracture. One can eliminate the constant properties (FFE, m, ρ, and C_p) by applying equation (14) to two different stress levels and measuring the steady-state temperatures for each case. Then, the following relationship can be used to determine the number of cycles to fatigue, N_{f_2}.

$$N_{f_2} = \frac{f_2}{f_1}\frac{T_{s_2}}{T_{s_1}}\frac{\theta_1^d}{\theta_2^d}N_{f_1} \tag{15}$$

To utilize equation (15) and construct the S-N curve, the following steps should be followed:

- Conduct a step-loading test to determine the fatigue limit and establish the relationship for the temperature rise due to non-damaging energies.
- Perform a fatigue test at any stress level above the fatigue limit, serving as the reference stress, until the material fractures. During this test, measure the steady-state temperature (T_{s_1}), the temperature rise at steady-state (θ_1^d), and the corresponding fatigue life (N_{f_1}).
- Conduct additional fatigue tests at various stress levels to reach steady-state conditions and measure the steady-state temperature (T_{s_2}) and temperature rise (θ_2^d) for each stress level. Alternatively, this step can be conducted using the step-loading method, where the test is continued at each stress level until reaching steady-state conditions, allowing for the measurement of steady-state temperatures at each stress level.
- Utilize equation (15), along with the known frequencies and stress levels, to calculate the fatigue life at the desired stress level.

The findings derived from this methodology are outlined in "Construction of S-N Curves" section, encompassing multiple materials.

Experiments and Methods

To assess the efficacy of the proposed approach, a set of fatigue tests at different stress amplitudes was performed on Carbon Steel (CS) 1018 and Stainless Steel (SS) 316. Next, the material composition, test method, equipment, and experimental procedure are described.

Material and Test Equipment

The chemical composition, physical, and mechanical properties of CS 1018 and SS316 are shown in Tables 1 and 2. Figure 3 shows the monotonic tensile test results for these materials. Specimens are cylindrical dog-bone shaped and are manufactured based on ASTM E 466-15 for fatigue testing. The specimens' surfaces are polished to remove stress concentration. The gauge sections of specimens are sprayed with a black paint layer to increase the thermal emissivity. Figure 4 shows the designed and painted specimens.

As shown in Fig. 5, the fatigue tests are conducted using a testing machine that can handle a maximum axial load of 25 kN. To prevent any slipping between the specimens and the gripping jaws of the machine, the tail ends of the specimens are securely held with appropriate gripping pressure. The strain of specimens is measured using a high-temperature extensometer which records the data at a rate of 250 Hz. In order to monitor the surface temperature changes during the fatigue tests, an infrared (IR) camera is employed. This IR camera is capable of capturing temperatures ranging

Table 2 Mechanical, physical, and thermal properties of CS 1018 and SS 316

Material	Density (ρ)	Thermal conductivity (k)	Specific heat capacity (C)	Young's modulus (E)	Ultimate Strength (σ_u)	Yield strength (σ_y)
	(Kg/m^3)	(W/m.K)	(J/kg.K)	GPa	MPa	MPa
CS 1018	7870	51	486	203	728	407
SS 316	7880	16.3	490	171	640	335

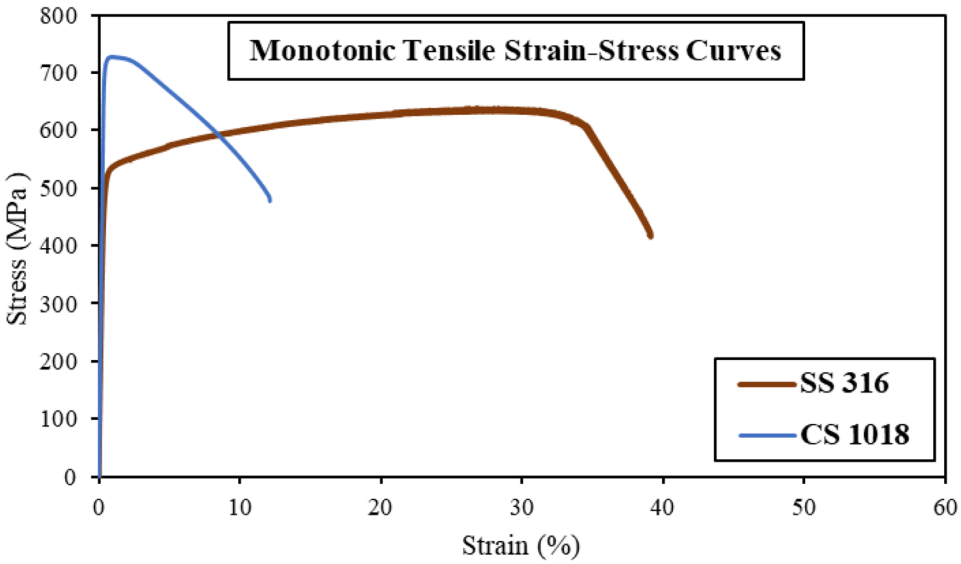

Fig. 3 Monotonic tensile test results for CS 1018 and SS 316

from 0 °C to 500 °C with a sensitivity of 0.08 °C at 30 °C, an accuracy of ± 2% of the reading, and a resolution of 320×240 pixels.

Test Procedure and Thermography Data Processing

Uniaxial load-controlled fatigue tests are carried out at different stress levels to obtain the steady-state temperature. The tests are performed at a load ratio of -1 and frequency of 10 Hz. The testing process involves two initial repetitions for each test case to assess data consistency. If significant data scatter is observed, additional repetitions are introduced to improve reliability. Referring to Fig. 1, the specimens at ambient temperature are subjected to the fatigue load to reach steady-state (Phase II) and the tests are continued to final failure.

As explained in "Life Prediction Using Temperature Rise" section, the assessment of the non-damaging part of energy dissipation at stress levels above the fatigue limit necessitates the determination of the fatigue limit for the materials. To achieve this, we devised a step-loading procedure aimed at applying the load in specific intervals while monitoring the temperature evolution during fatigue loading. The initial load was set at 200 MPa, a value significantly below the yield strength of both materials. Throughout the step-loading process, intervals of 25 MPa were employed for load increments. However, as we approached load levels near the fatigue limit, we refined the step intervals to enhance the accuracy of our predictions.

In this work, we assumed that the temperature rise originates from inelastic, anelastic, and thermoelastic effects [32]. The damaging part of energy, caused by microplasticity and changes in microstructure that increase the mean temperature, is referred to as the inelastic effect. On the other hand, the non-damaging part of the energy, resulting from internal friction and also contributing to the mean temperature rise, is known as the anelastic effect. Additionally, the thermoelastic effect causes temperature fluctuations around the mean temperature but does not alter the temperature at the end of each cycle. Thus, the mean temperature is utilized in this paper to assess the dissipation of both damaging and non-damaging energy components. It should be noted that the temperature of the fracture zone in the gauge section which is the hottest part of the specimen is used for analysis. To ensure the accuracy and reliability of the mean temperature values, we have selected a data acquisition rate of 50 Hz for the IR camera, which is five times the loading frequency. This high acquisition rate allows us to capture temperature variations with greater precision and effectively analyze thermal behavior during the testing process.

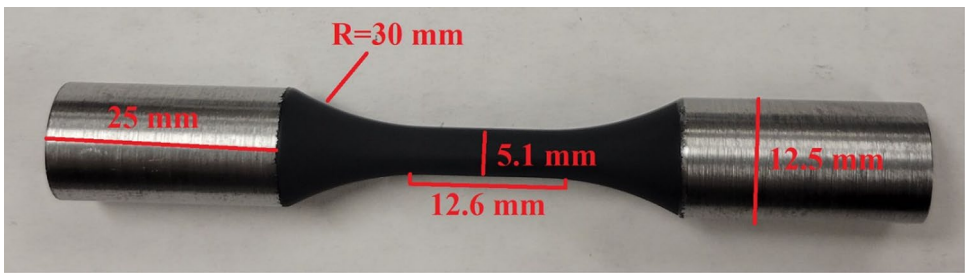

Fig. 4 Dimensions of painted fatigue specimen

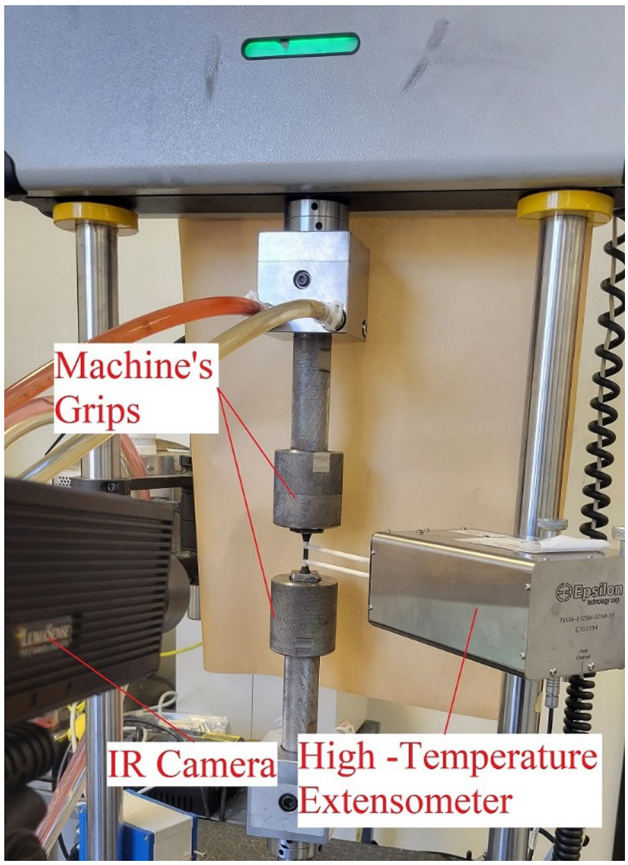

Fig. 5 Fatigue test set-up

The steady-state temperatures are measured when the fatigue reaches the stabilization stage. The temperature stabilizes after a few minutes, thus the change in ambient temperature is negligible compared to the temperature rise in the specimens. In order to eliminate the noise signals associated with the ambient temperature, the ambient temperature (temperature of the machine's grips) was subtracted from the mean temperature value, allowing us to obtain the pure temperature rise during fatigue. However, to account for possible fluctuations in temperature due to changes in the surrounding conditions or potential misreading from the camera, we take the average of the mean temperature over a 10-s interval as the representative mean temperature during fatigue. This approach helps to mitigate any potential inaccuracies in our temperature measurements to obtain the accurate values of mean temperature.

Results and Discussion

This section uses temperature measurements to obtain the fatigue life of CS 1018 and SS 316 specimens undergoing tension-compression cyclic loading. In addition, the experimental data available in the literature for other materials and testing conditions are used to evaluate the efficacy of the proposed method. In "Fatigue Limit" section the trends of temperature rise during fatigue at different stress levels for CS 1018 and SS 316 are presented to obtain the fatigue limit. "Construction of S-N Curves" section shows how the entropic concept can be utilized to construct the S-N curve for different materials using only a few specimens.

Fatigue Limit

Once the fatigue test begins, the temperature of the component undergoing cyclic loading increases rapidly due to the initial loading. As the fatigue loading continues, the rate of temperature rise decreases, and the temperature eventually reaches a steady-state condition during phase II of the test. Figure 6 provides a visual representation of the surface

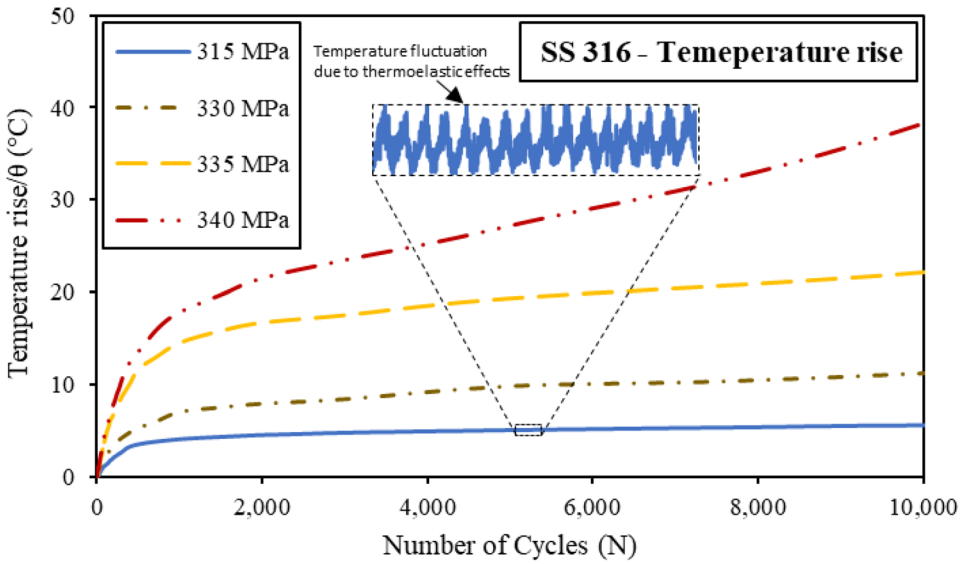

Fig. 6 Temperature profiles of SS316 during initial stages of fatigue at different stress levels

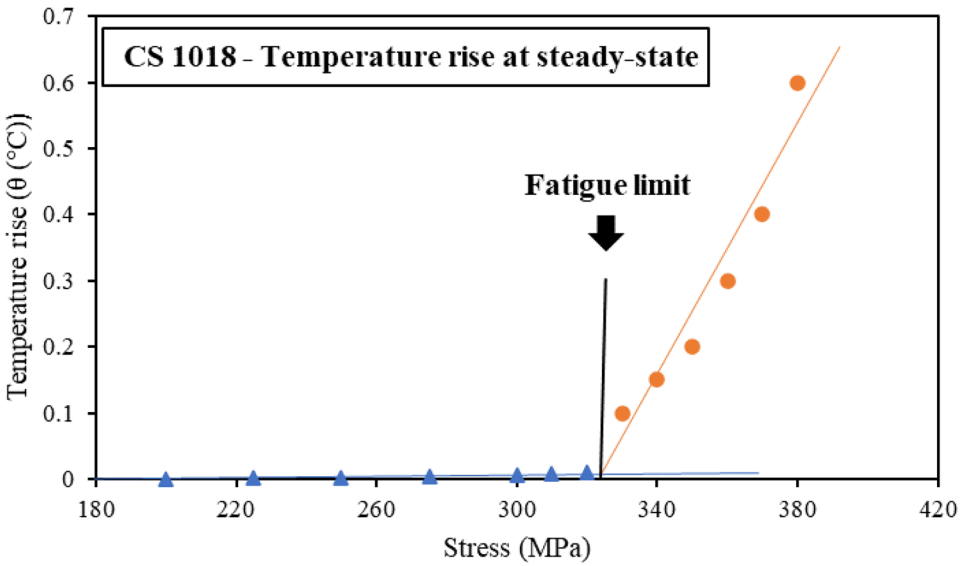

Fig. 7 Obtaining the fatigue limit of CS 1018 based on temperature rise at steady-state [31]

temperature of the SS 316 specimens as it progressively increases at different stress levels during the first phase and ultimately reaches a steady state during the second phase.

The temperature exhibits fluctuations around the mean value, primarily due to the thermoelastic effect. To enhance the accuracy of our measurements, we adopted a method to calculate the mean value. Specifically, we computed the average of mean values recorded over 10-s intervals during the second phase of the test. This approach allowed us to reduce the impact of short-term variations and provide a more precise estimation of the mean temperature during the steady-state condition.

Referring to Fig. 2, the fatigue limit is used to distinguish between the damaging and non-damaging energies in cyclic loading. For fatigue cases below the fatigue limit, the energy distribution can be attributed to the internal friction and non-damaging source of energy, such as recoverable dislocations in material structure. The fatigue process encompasses a combination of plastic, elastic, and anelastic deformations. Internal friction is a non-damaging phenomenon arising from inherent flaws in the form of half-planes that can move within the material's lattice during repeated loading. When subjected to cyclic loading, the applied stress supplies sufficient activation energy for these half-planes to undergo edge dislocations. The gradual transition of these kink bands restores them to their initial positions, resulting in no damage [34]. This non-damaging, recoverable concept contributes to heat generation and temperature rise during cyclic loading, even at stress levels below the fatigue limit.

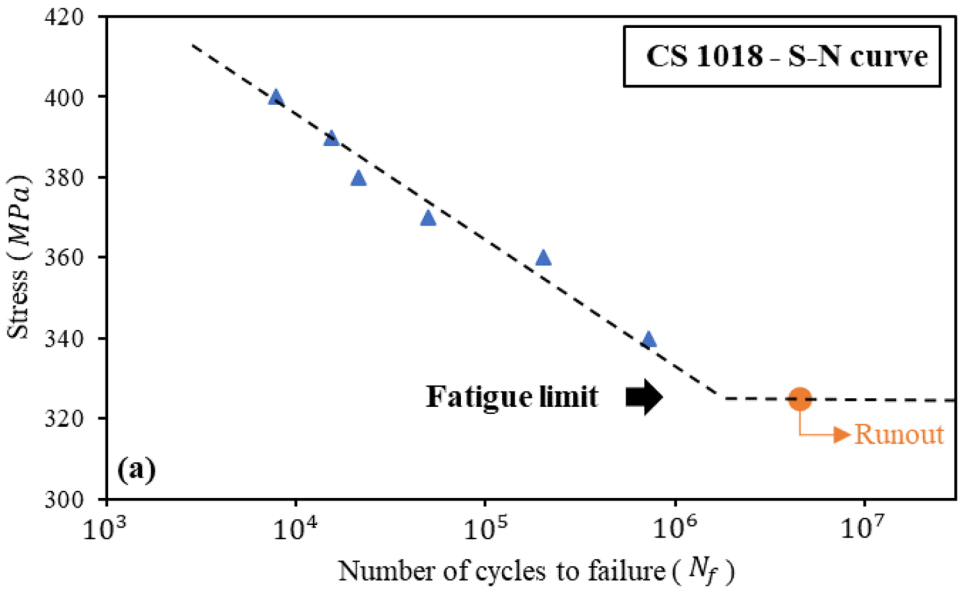

Fig. 8 S-N curve of CS 1018 [31]

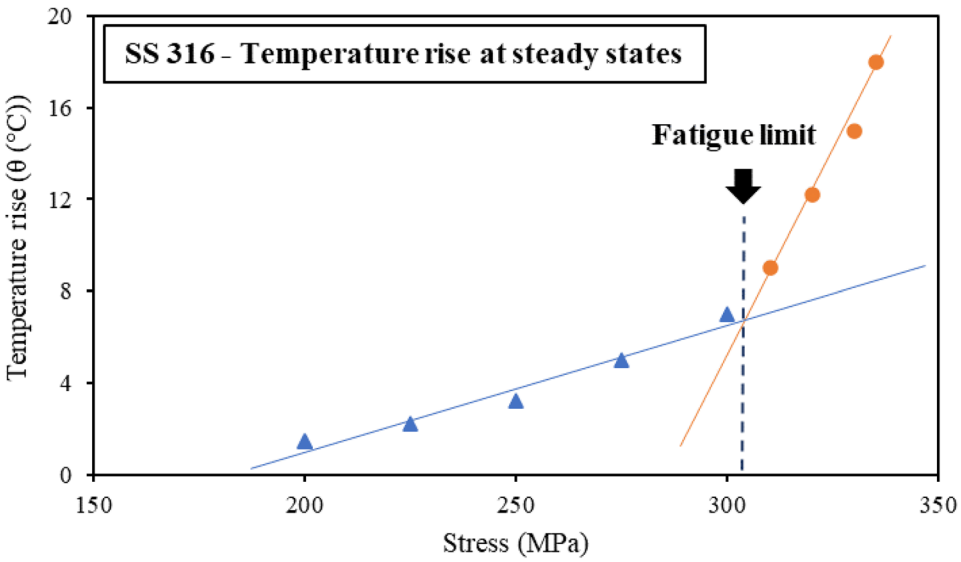

Fig. 9 Obtaining the fatigue limit of SS 316 based on temperature rise at steady-state

In this study, only the temperature rise due to damaging energies (θ^d) are used to find the fatigue life. Figure 7 shows the temperature rise for CS 1018 specimens at different stress levels [31]. For stress levels below the fatigue limit the temperature rise is almost zero and the steady-state temperature is obtained using the average mean values of steady-state temperature. The obtained fatigue limit is 325 MPa, which agrees with the S-N curve data presented in Fig. 8. Figure 9 also shows the steady-state temperature rise at different stress levels for SS 316. This demonstrates that even at low stress levels, a significant amount of temperature rise occurs due to internal friction. However, for stress levels exceeding 310 MPa, there is a notable spike in temperature rise at the same stress intervals, signifying that the fatigue limit of the material is 310 MPa. It is in good agreement with the S-N curve results of SS316 presented in Fig. 10. In Fig. 8, the run-out point is associated with the fatigue test with 5,000,000 cycles without failure for CS 1018. Similarly, in Fig. 10, the test performed for 5,000,000 cycles, is also considered as the run-out for SS 316. The steady-state temperature rise in SS 316 is higher compared to CS 1018. This difference can be attributed to the higher amount of plastic strain energy released during fatigue loading and the lower heat conductivity of SS 316, which limits its heat dissipation capability. As a result, SS 316 experiences a more significant temperature increase in the steady state, reflecting its response to fatigue loading and material-specific characteristics.

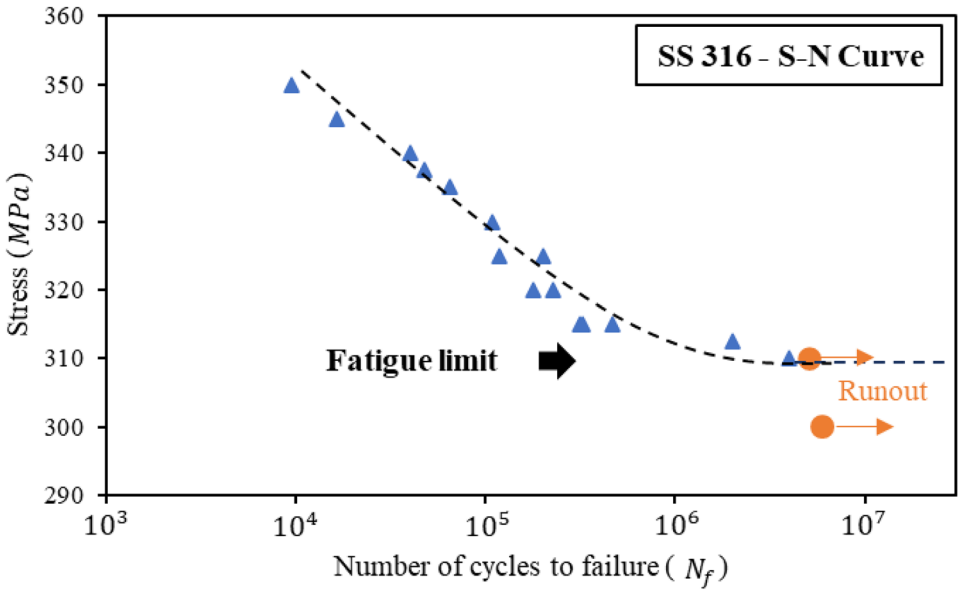

Fig. 10 S-N curve of SS 316

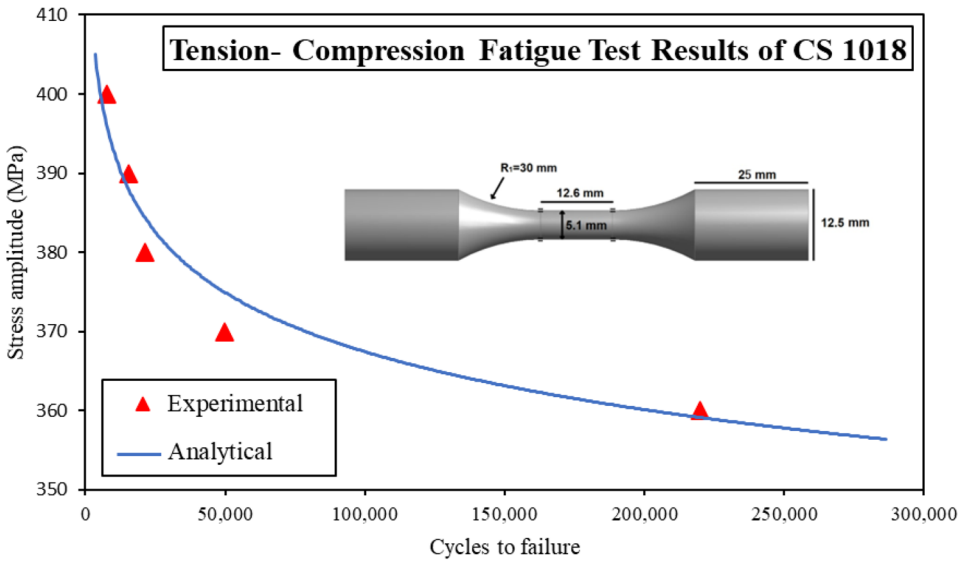

Fig. 11 Extracted S-N curve of CS 1018 based on the results of stabilized temperatures

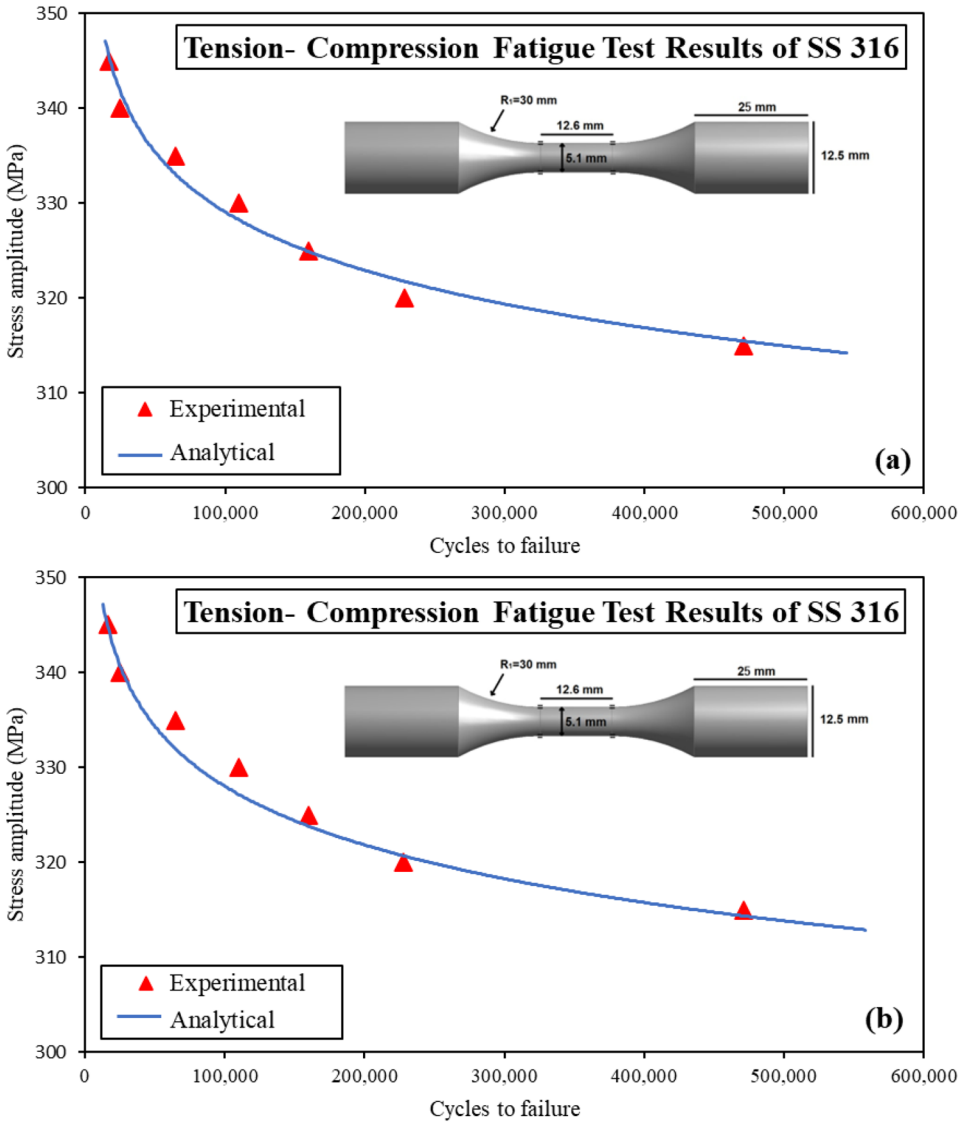

Fig. 12 Extracted S-N curve of SS 316 based on the results of stabilized temperatures with reference stress amplitude of (**a**) 330MPa and (**b**) 325 MPa

Construction of S-N Curves

Referring to equation (15), the S-N curve of a material can be obtained if the fatigue life and stabilized temperature at a stress level are determined. The stabilized temperature at another stress level can be used to find its corresponding fatigue life. The fatigue tests need to be carried out to reach Phase II of fatigue and obtain the steady-state temperature. In this study, it is assumed that fatigue life results of CS 1018 are available. The obtained temperature at the steady-state phase for other stress levels is used to find the corresponding fatigue life. Figure 11 shows the predicted results of this method in comparison with the experimental results for CS 1018. Also, Fig. 12 shows the predicted results for the fatigue life of SS 316 samples. To evaluate the model's predictions for SS 316, first assumed that the reference stress is 330 MPa, and the steady-state temperatures at other stress levels are used to construct the S-N curve. The results of this scenario are depicted in Fig. 12(a). For the second scenario, the stress amplitude of 325 MPa is assumed as reference stress, and the stabilized temperature of other stresses is used to Construct the S-N curve as shown in Fig. 12(b). For both cases, the predicted results have an acceptable correlation with the experiments. A summary of the results is presented in Table 3.

In addition to the experiments conducted in this study, the tension-compression fatigue results of the work of Teng et al. [35] on SAE 1045 medium carbon steel and fully-reversed bending fatigue results of the work of Mehdizadeh and Khonsari [28] are utilized to evaluate the merit of the proposed method.

In their study, Teng et al. [35] utilized thermography to investigate the fatigue behavior of SAE 1045 medium carbon steel. They conducted a series of step-wise tests ranging from 100 to 400 MPa, with a load step length of 9000 cycles for each stress level. Different load steps with values of $\Delta\sigma_a = 20$, 25, 30, 35, and 40 MPa were performed, and the temperature rise was measured for each load step. Additionally, constant amplitude load tests were carried out to obtain the S-N curve for the material. In this paper, we applied

Table 3 Model's predictions in comparison with the experimental results for various materials and load cases

Material	Loading type	Reference Load/ Displacement	Load Level	Estimated Life	Actual Life (Experiment)	Error (%)
CS 1018	Axial	380 MPa	360 MPa	256500	219800	16.6
			370 MPa	51300	49900	2.9
			390 MPa	12900	15300	-15.6
			400 MPa	6500	7800	-16.7
SS 316	Axial	330 MPa	315 MPa	464700	471100	-1.3
			320 MPa	282500	228300	23.9
			325 MPa	182200	160200	13.8
			335 MPa	46900	64500	-27.2
			340 MPa	25900	25000	3.7
			345 MPa	21200	16500	28.8
SS 316	Axial	330 MPa	315 MPa	408100	471100	-13.3
			320 MPa	248100	228300	8.8
			330 MPa	96600	110300	-12.1
			335 MPa	41200	64500	-36.1
			340 MPa	22800	25000	-8.9
			345 MPa	18700	16500	13.1
SAE 1045	Axial	350 MPa	300 MPa	387000	279300	-27.8
			320 MPa	159000	114700	-27.8
			325 MPa	113200	81600	-27.7
			340 MPa	76600	55300	-22.1
			360 MPa	48100	34700	23.9
			380 MPa	30100	20100	34.1
			400 MPa	15100	10900	20.8
SS 304	Bending	8.9 mm	6.3 mm	1545200	2450700	-36.9
			7 mm	755700	755200	0.1
			7.6 mm	401200	394900	1.6
			10 mm	133200	109800	21.1
			11.5 mm	111200	84500	32.3

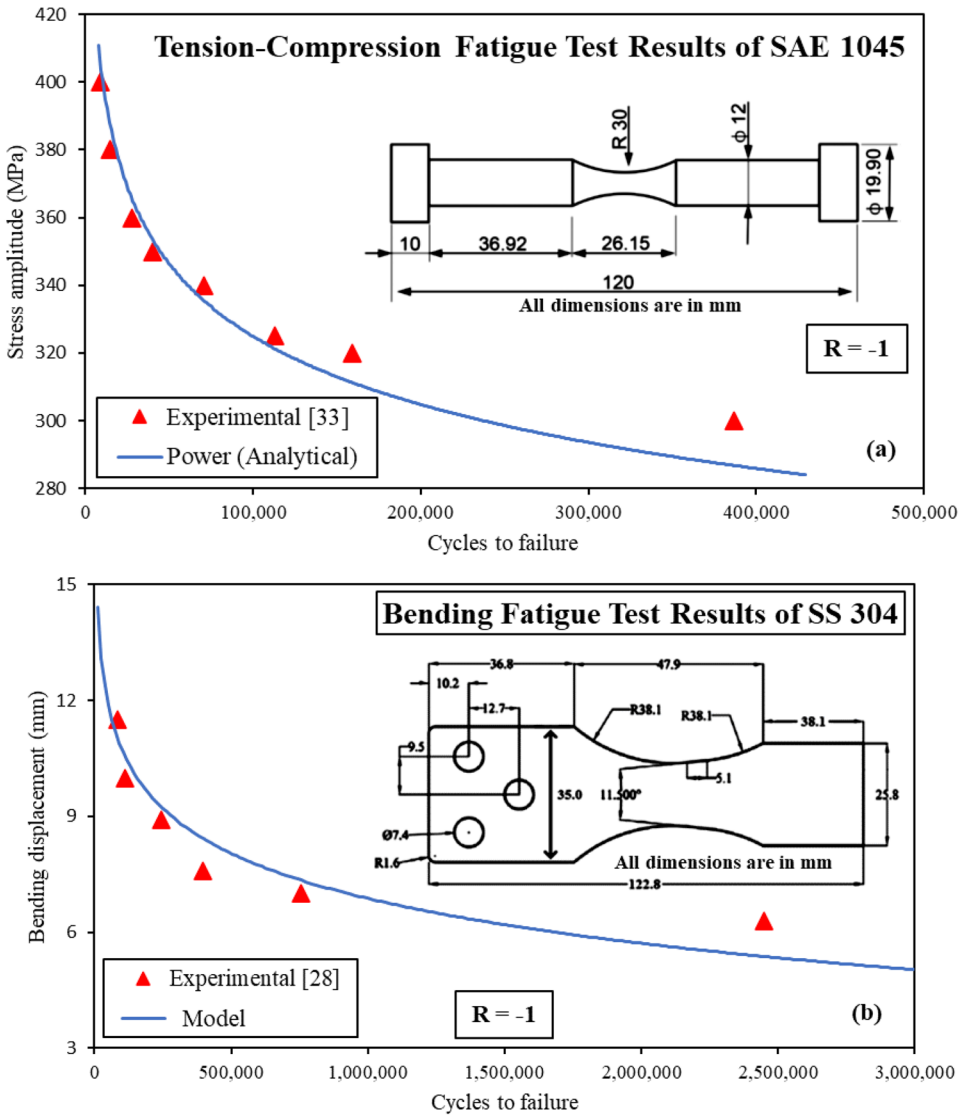

Fig. 13 Extracted S-N curve of (**a**) SAE 1045 and (**b**) SS 304 in comparison with the experimental results available in Refs. [28, 35]

the proposed method to their experimental results to construct the S-N curve. For the construction of the S-N curve, a stress amplitude of 350 MPa was chosen as the reference stress since the fatigue limit is approximately 300 MPa. The comparison of the predicted and experimental S-N curves for SAE 1045 steel is depicted in Fig. 13(a) and results are summarized in Table 3.

In another study, Mehdizadeh and Khonsari [28] conducted a series of fully-reversed bending fatigue tests on SS 304 to investigate the influence of internal friction on temperature evolution during low and high-cycle fatigue tests. They applied displacements ranging from $\Delta l = 4$ to 12 mm and measured the corresponding temperature evolution. Additionally, they obtained the fatigue life corresponding to each displacement. In this paper, we utilized the developed method to analyze their experimental results and predict the S-N curve for SS 304. To achieve this, we used the life and temperature rise data obtained at a displacement of 8.9 mm as a reference to predict fatigue life at other stress levels. Figure 13(b) and Table 3 illustrate the estimated results for SS 304 under fully-reversed bending tests, showing the predicted S-N curve based on the applied method and the experimental data obtained from the tests performed by Mehdizadeh and Khonsari [28].

As shown in Fig. 13, the predicted results for both low- and high-cycle fatigue are in good agreement with the experiments. It shows that this concept provides a simple yet powerful method to rapidly extract the S-N curves of different materials under different types of fatigue loads.

Conclusions

An experimentally verified procedure is proposed to rapidly predict fatigue life by measuring the temperature rise during the fatigue process. Based on the presented experimental results, the stabilized temperature during cyclic loading is an indicator of internal heat generation and can be utilized to measure the plastic strain energy. Furthermore, the results show that the measure of stabilized temperature can provide a simple, reliable, and efficient methodology based on the framework of entropy accumulation to find the S-N curve for material by only carrying out the experiments until reaching the steady-state temperature.

The results presented indicate the versatility of this approach in handling various types of fatigue loading, such as axial tension-compression and bending. With only a few specimens for each loading type, one can characterize the fatigue behavior of a material and develop the S-N curve. This approach offers a time- and cost-efficient solution that is both effective and reliable.

Funding This work is supported in part by the members of the Center for Innovations in Structural Integrity Assurance (CISIA) under the US National Science Foundation award number 2052810. Also, the lead author (A.M.) wishes to acknowledge that the research was supported in part by the Louisiana Experimental Program to Stimulate Competitive Research (EPSCoR), funded by the National Science Foundation and the Board of Regents Support Fund under Cooperative Agreement Number OIA-1946231 (CFDA # 47.083).

Declarations

Conflicts of Interest The Authors declare to have no conflicts of interest.

References

1. Ye X, Su Y, Han J (2014) A state-of-the-art review on fatigue life assessment of steel bridges. Math Probl Eng 2014:1–13
2. Meneghetti G (2007) Analysis of the fatigue strength of a stainless steel based on the energy dissipation. Int J Fatigue 29(1):81–94
3. Huang Y, Li S, Lin S, Shih C (1984) Using the method of infrared sensing for monitoring fatigue process of metals. Mater Eval 42(8):1020–1024
4. Amiri M, Khonsari M (2010) Life prediction of metals undergoing fatigue load based on temperature evolution. Mater Sci Eng A 527(6):1555–1559
5. Luong MP (1995) Infrared thermographic scanning of fatigue in metals. Nucl Eng Des 158(2–3):363–376
6. Boulanger T, Chrysochoos A, Mabru C, Galtier A (2004) Calorimetric analysis of dissipative and thermoelastic effects associated with the fatigue behavior of steels. Int J Fatigue 26(3):221–229
7. Morabito A, Chrysochoos A, Dattoma V, Galietti U (2007) Analysis of heat sources accompanying the fatigue of 2024 T3 aluminium alloys. Int J Fatigue 29(5):977–984
8. Chrysochoos A, Huon V, Jourdan F, Muracciole JM, Peyroux R, Wattrisse B (2010) Use of full-field digital image correlation and infrared thermography measurements for the thermomechanical analysis of material behaviour. Strain 46(1):117–130
9. Jiang L, Wang H, Liaw P, Brooks C, Klarstrom D (2001) Characterization of the temperature evolution during high-cycle fatigue of the ULTIMET superalloy: experiment and theoretical modeling. Metall Mater Trans A 32(9):2279–2296
10. Fargione G, Geraci A, La Rosa G, Risitano A (2002) Rapid determination of the fatigue curve by the thermographic method. Int J Fatigue 24(1):11–19
11. Amiri M, Khonsari M (2010) Rapid determination of fatigue failure based on temperature evolution: Fully reversed bending load. Int J Fatigue 32(2):382–389
12. La Rosa G, Risitano A (2000) Thermographic methodology for rapid determination of the fatigue limit of materials and mechanical components. Int J Fatigue 22(1):65–73
13. Guglielmino E, Risitano G, Santonocito D (2019) A new approach to the analysis of fatigue parameters by thermal variations during tensile tests on steel. Procedia Structural Integrity 24:651–657
14. Palumbo D, Galietti U (2014) Characterisation of steel welded joints by infrared thermographic methods. Quant Infrared Thermogr J 11(1):29–42
15. De Finis R, Palumbo D, Ancona F, Galietti U (2015) Fatigue limit evaluation of various martensitic stainless steels with new robust thermographic data analysis. Int J Fatigue 74:88–96
16. Fatemi A, Yang L (1998) Cumulative fatigue damage and life prediction theories: a survey of the state of the art for homogeneous materials. Int J Fatigue 20(1):9–34
17. Basaran C, Yan CY (1998) A thermodynamic framework for damage mechanics of solder joints. ASME J Electron Packag 120(4):379–384
18. Naderi M, Khonsari M (2010) A thermodynamic approach to fatigue damage accumulation under variable loading. Mater Sci Eng A 527(23):6133–6139
19. Ontiveros V, Amiri M, Kahirdeh A, Modarres M (2017) Thermodynamic entropy generation in the course of the fatigue crack initiation. Fatigue Fract Eng Mater Struct 40(3):423–434
20. Mahmoudi A, Mohammadi B (2019) On the evaluation of damage-entropy model in cross-ply laminated composites. Eng Fract Mech 219:106626
21. Huang J, Li C, Liu W (2020) Investigation of internal friction and fracture fatigue entropy of CFRP laminates with various stacking sequences subjected to fatigue loading. Thin-Walled Structures 155:106978
22. Amiri M, Modarres M (2014) An entropy-based damage characterization. Entropy 16(12):6434–6463
23. Naderi M, Amiri M, Khonsari M (2010) On the thermodynamic entropy of fatigue fracture. Proc Math Phys Eng Sci 466(2114):423–438
24. Mahmoudi A, Mohammadi B (2019) Theoretical-experimental investigation of temperature evolution in laminated composites due to fatigue loading. Compos Struct 225:110972
25. Lemaitre J, Chaboche JL (1994) Mechanics of solid materials. Cambridge University Press
26. Halford G (1966) The energy required for fatigue(Plastic strain hystersis energy required for fatigue in ferrous and nonferrous metals). J Mater 1:3–18
27. Naderi M, Khonsari M (2012) A comprehensive fatigue failure criterion based on thermodynamic approach. J Compos Mater 46(4):437–447
28. Mehdizadeh M, Khonsari M (2018) On the role of internal friction in low-and high-cycle fatigue. Int J Fatigue 114:159–166
29. Jang J, Khonsari M (2018) On the evaluation of fracture fatigue entropy. Theoret Appl Fract Mech 96:351–361

30. Mahmoudi A, Khonsari MM (2022) Entropic Characterization of Fatigue in Composite Materials. Encyclopedia of Materials: Plastics and Polymers: Elsevier (vol. 2, pp. 147–162)
31. Mahmoudi A, Khonsari MM (2023) Rapid evaluation of fatigue limit using energy dissipation. Fatigue Fract Eng Mater Struct 46(6):2156–2167
32. Yang W, Guo X, Guo Q, Fan J (2019) Rapid evaluation for high-cycle fatigue reliability of metallic materials through quantitative thermography methodology. Int J Fatigue 124:461–472
33. Haghshenas A, Jang J, Khonsari M (2021) On the intrinsic dissipation and fracture fatigue entropy of metals. Mech Mater 155:103734
34. Guo Q, Zairi F, Yang W (2020) Evaluation of intrinsic dissipation based on self-heating effect in high-cycle metal fatigue. Int J Fatigue 139:105653
35. Teng Z, Wu H, Boller C, Starke P (2020) Thermography in high cycle fatigue short-term evaluation procedures applied to a medium carbon steel. Fatigue Fract Eng Mater Struct 43(3):515–526

Publisher's Note Springer Nature remains neutral with regard to jurisdictional claims in published maps and institutional affiliations.

Springer Nature or its licensor (e.g. a society or other partner) holds exclusive rights to this article under a publishing agreement with the author(s) or other rightsholder(s); author self-archiving of the accepted manuscript version of this article is solely governed by the terms of such publishing agreement and applicable law.